Computational Modeling of the Fluid Mechanical Environment of Regular and Irregular Scaffolds

Liu-Lan Lin   Yu-Jie Lu   Ming-Lun Fang

School of Mechatronics Engineering and Automation, Shanghai University, 99 Shangda Road, Shanghai 200444, China

Abstract: Direct perfusion of three-dimensional cell-seeded biological scaffolds is known to enhance osteogenesis, which can be partly attributed to mechanical stimuli affecting cell proliferation and differentiation in the process of bone tissue regeneration. This study aimed to compare the hydrodynamic environment, including the distributions of fluid flow velocity, wall shear stress and pressure in pores filled with liquid, designed scaffold (DS), porous and biodegradable β-TCP (β-tricalcium phosphate) based on freeze-drying scaffold (FS) and dog′s femora scaffold (NS). Gravity condition, inlet velocities of 1, 10, 100 and 1000 μm/s and medium viscosities of 1.003, 1.45 and 2.1 mPas were applied as the initial conditions. With an inlet fluid velocity of 100 m/s and a viscosity of 1.45 (10^{-3} Pas, the simulation results of maximal and average wall shear stress were 15.675 mPas and 3.223 mPas for DS, 67.126 mPas and 5.949 mPas for FS, and 20.190 mPas and 1.629 mPas for NS. Variations of inlet fluid velocity and fluid viscosity produced corresponding proportional changes in fluid flow velocity, wall shear stress and pressure. DS and FS were evaluated in terms of simulation results and microstructure using NS as a reference standard. This methodology allows a greater insight into the complex concept of tissue engineering and will likely help in understanding and eventually improving the fluid-mechanical aspects.

Keywords: Scaffold, perfusion, micro-CT, computational fluid dynamics (CFD), wall shear stress.

1 Introduction

Most fractures heal uneventfully. However, between 5 % and 10 % of them result in nonunion[1]. Large bone defects with a size of over 3 mm generally do not naturally heal, which presents a clinical challenge. The growing demand for bone grafts has led surgeons to investigate more advanced techniques for reconstruction of bone defects. Tissue engineering may be a promising alternative to conventional treatments. One commendable approach was to culture mesenchymal stem cells in vitro within a biomaterial scaffold to produce a bone-like layer of tissue[2−4]. Then, the engineered bone tissue is implanted into the body to reconstruct large bone defects. Although promising results have been obtained for the healing of large bone defects[5], much more research is needed before the bone engineering can enter daily clinical practice.

The cultivation of tissue constructs in vitro and static conditions, typically result in an outer shell of viable cells, while the inner core becomes necrotic due to the poor diffusive delivery of nutrients and the accumulation of wastes[6]. A bioreactor system has been developed to generate dynamic fluid perfusion within cell-seeded scaffolds, and it was found to have beneficial effects on cell function and the growth of bone tissue[7−11]. Compared to static controls, the improvement of mass transport and nutrient exchange

in bioreactor systems can increase cell viability and extracellular matrix formation[12, 13]. Meanwhile, cell response was associated with the fluid flow velocity and wall shear stress in perfusion configurations[14].

Although there is a clear relationship between macroscopic mechanical loads and tissue differentiation, it is difficult to determine the local mechanical stimuli sensed by the cells at a microscopic level. Fluid flow velocity and wall shear stress distributions within a scaffold at a microscopic level can be obtained by using the computational fluid dynamics (CFD) method. Different types of mechanical stimuli have been considered for the prediction of tissue formation[15−18].

Others have used computer-aided design approaches where scaffolds were built as a repeat pattern of unit cells[11, 19]. This method allows proper actual estimation results of fluid flow velocity, wall shear stress and pressure within the model which can be used for easy manufacture. However, a more realistically geometric representation of a scaffold was obtained through micro-computed tomography (micro-CT). Combined with the CFD method, more accurate results will be achieved to indicate the natural distributions of fluid flow velocity, wall shear stress and pressure.

The main goal of this study was to build CFD models to obtain detailed information of the interstitial fluid velocity, wall shear stress and pressure within the pores of three scaffolds for several initial conditions, and to assess the microstructure and fluid simulation results of these three models with given initial conditions.

(a) Designed scaffold   (b) Freeze-drying scaffold   (c) Dog femora scaffold
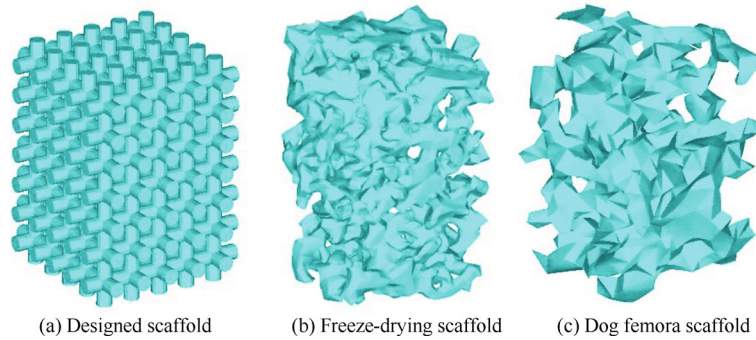
Fig. 1   CAD models of 3 types of scaffolds

2   Materials and methods

In this study, we used a designed scaffold (DS) model and the size was $2.2\,\mathrm{mm} \times 2.2\,\mathrm{mm} \times 3\,\mathrm{mm}$, as shown in Fig. 1 (a). The diameter of the canal was $0.2\,\mathrm{mm}$, and the gap of the canal was $0.2\,\mathrm{mm}$. Two other scaffolds approximately $2\,\mathrm{mm}$ in length, $2\,\mathrm{mm}$ in width and $3\,\mathrm{mm}$ in height with different morphologies were used, as shown in Fig. 1 (b)(freeze-drying scaffold, FS) and (c) (dog femora scaffold, NS). These two samples were scanned using a MicroCT80 with a resolution of $20\,\mu\mathrm{m}$. Computer reconstruction of these samples in three dimensions was made using Mimics, as shown in Fig. 2.
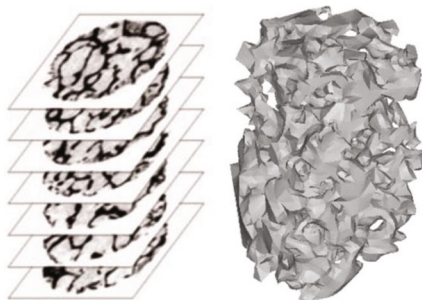
Fig. 2   Procedure from micro-CT images to model selection shown for natural bone scaffold

The fluid phase was obtained by subtracting the scaffold from a chamber (DS: $2.6\,\mathrm{mm} \times 2.6\,\mathrm{mm} \times 3.4\,\mathrm{mm}$; FS: $2.5\,\mathrm{mm} \times 2.5\,\mathrm{mm} \times 4\,\mathrm{mm}$;   NS: $3.1\,\mathrm{mm} \times 3.1\,\mathrm{mm} \times 4\,\mathrm{mm}$), as shown in Fig. 3.

Three-dimensional (3D) tetrahedral meshes for the domains include the interconnected pores and the perfusion chamber which were made in HyperMesh with an element size of $50\,\mathrm{mm}$, as shown in Fig. 4. There were $1\,050\,000$ elements made for DS, $820\,000$ elements made for FS and $1\,150\,000$ elements made for NS. The size of the osteocyte adhering to the surface of the scaffold was about $50\,\mathrm{mm}$. Consequently, seven boundary layers (the first minimum layer thickness was $0.002\,\mathrm{mm}$) based on a growth ratio of 1.2 on the surface of the scaffold models which cell mainly perch were made to capture the distribution of fluid flow velocity and wall shear stress, as shown in Fig. 4.

The analysis was carried out by using fluid. The outlet fluid pressure was set as zero, and these surfaces of the scaffolds were set as no-slip walls. Operating pressure was $101\,325\,\mathrm{Pa}$, while gravitational acceleration was $9.8\,\mathrm{m/s^2}$. The culture medium was modeled as an incompressible and homogeneous Newtonian fluid with a density of $1\,000\,\mathrm{kg/m^3}$, as shown in Fig. 5. Four levels of inlet velocity and three levels of fluid viscosity were used to make up 36 different cases, as shown in Table 1. Fluid flow velocity, wall shear stress and pressure were calculated.

3   Results

Fluid flow velocities for DS, FS and NS were calculated at 4 levels of inlet velocity and 3 levels of fluid viscosity. The maximal and average velocities are presented in Table 2.

(a) Fluid phase of DS   (b) Fluid phase of FS   (c) Fluid phase of NS
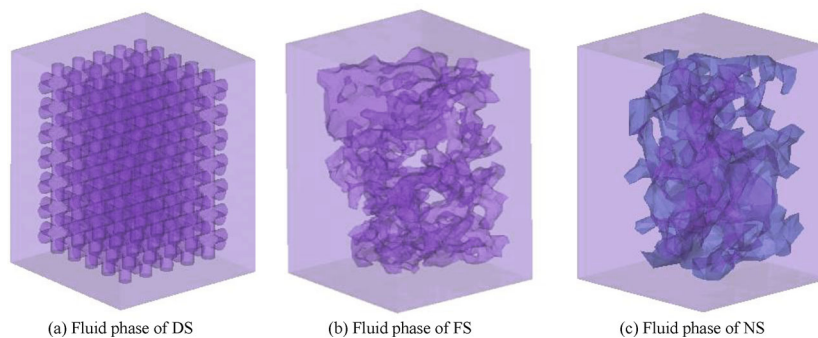
Fig. 3   The structure diagram of the algorithm

(a) 1 050 000 elements for DS   (b) 820 000 elements for FS   (c) 1 150 000 elements for NS   (d) Boundary layers
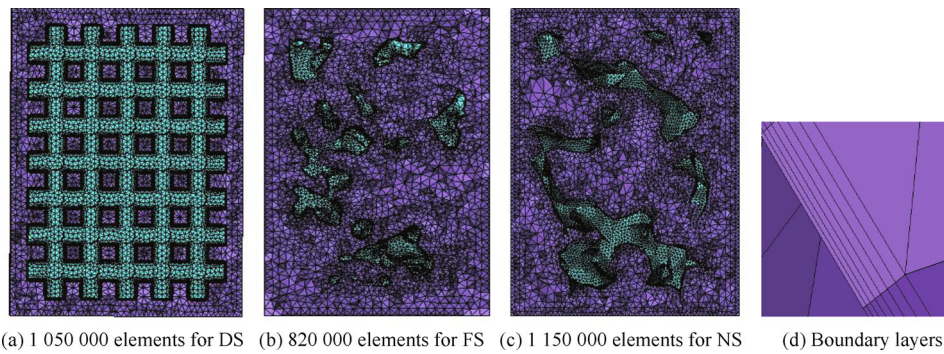
Fig. 4   Meshes for DS, FS and NS

(a) Inlet velocity of DS   (b) Inlet velocity of FS   (c) Inlet velocity of NS
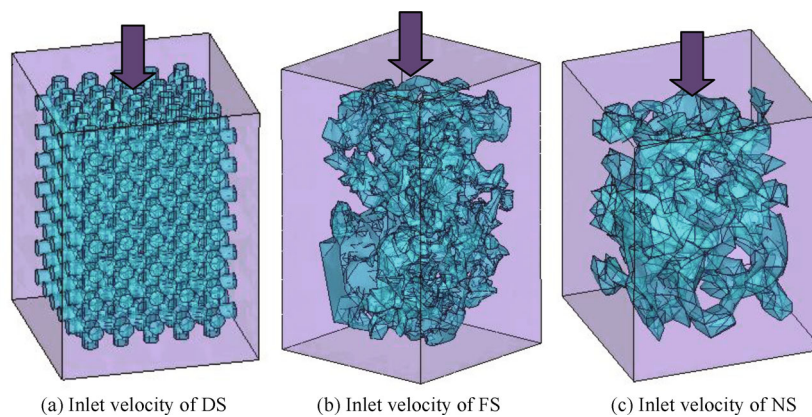
Fig. 5   Inlet velocity of DS, FS and NS

For the same scaffold, with the viscosity increasing, the maximal and average fluid flow velocity decreased correspondingly and slightly for each value of inlet velocity. The viscosity had a limited impact on the fluid flow velocity. The fluid flow velocity increased correspondingly as the inlet velocity increased. The fluid flow velocity remained about 2 to 4 times the inlet velocity. At the same inlet velocity and viscosity, the maximal fluid flow velocity appeared for DS. The maximal fluid flow velocity in DS was nearly more than 172% of FS and NS′s velocity (initial conditions: inlet velocity was $10\,\mathrm{m/s}$ and viscosity was $2.1 \times 10^{-3}\,\mathrm{Pas}$, DS: $42.535\,\mu\mathrm{m/s}$, FS: $15.618\,\mu\mathrm{m/s}$ and NS: $18.868\,\mu\mathrm{m/s}$), while the average velocity was more than 440% of FS and NS′s velocity (initial conditions: inlet velocity was $10\,\mu\mathrm{m/s}$ and viscosity was $2.1 \times 10^{-3}\,\mathrm{Pas}$, DS: $13.246\,\mu\mathrm{m/s}$, FS: $2.454\,\mu\mathrm{m/s}$ and NS: $2.867\,\mu\mathrm{m/s}$). At the same initial conditions, the maximal and average fluid flow velocities in FS were a little more than those in NS. From this it can be considered that FS had a more reasonable microscopic structure than DS. The microscopic structure of FS was closer to that of the real scaffold (NS).

From Fig. 6, it is observed that the maximal and average fluid flow velocities in FS were closer to those in NS than in DS. The biggest difference was concentrated in the inlet velocity range between $10\,\mu\mathrm{m/s}$ and $100\,\mu\mathrm{m/s}$. Relevant studies showed that it was quite useful for the cultivation of cell-seeded scaffold in a bioreactor. So FS was more suitable instead of natural bone than DS from the point of view of fluid flow velocity.

Wall shear stresses for DS, FS and NS were calculated at 4 levels of inlet fluid velocity and 3 levels of fluid viscosity. The maximal and average wall shear stresses are presented in Table 3.

As the inlet velocity increased, the maximal and average wall shear stresses increased correspondingly. At the same inlet velocity and viscosity, wall shear stresses showed mainly a linear relationship, as shown in Fig. 7. Although increased viscosity reduced the fluid flow velocity, the wall shear stress increased, which indicated that the influence of viscosity on the wall shear stress was greater than that of the inlet velocity within a certain region. For the condition of inlet velocity of $100\,\mu\mathrm{m/s}$ and viscosity of $1.45\times10^{-3}\,\mathrm{Pas}$, the maximal and average wall shear stresses were $15.675\,\mathrm{mPas}$ and $3.223\,\mathrm{mPas}$ in DS, $67.126\,\mathrm{mPas}$ and $5.949\,\mathrm{mPas}$ in FS, and $20.190\,\mathrm{mPas}$ and $1.629\,\mathrm{mPas}$ in NS. From Fig. 8, the maximal and average wall shear stresses in FS were lower than in DS except for these results obtained at an inlet velocity of $10\,\mu\mathrm{m/s}$. The wall shear stress was not consistent in FS and NS. This was explained by the fact that the pores were so small in FS that the distribution of wall shear stress was greatly affected.

Table 1   Levels of fluid viscosity and inlet fluid velocity used for CFD simulation

OPP	CSU:OPP	Group decision (%)	Unit decision (%)	Group decision/unit decision
Cyberoos2001	3:0	71.5	28.5	2.51
FCPortugal2001	1:0	68.4	31.6	2.16
Gemini	26:0	59.7	40.3	1.48
Harmony	3:0	69.9	30.1	2.32
Lazarus	11:0	57.3	42.7	1.34
MRB	2:0	63.2	32.8	1.93
SBCe	4:1	65.8	34.2	1.92
UvA_Trilearn_2001	1:0	54.9	44.1	1.24
UTUtd	10:0	70.7	29.3	2.41
WrightEagle2001	3:1	66.2	33.8	1.96
Average		64.8	35.2	1.84

Table 2   Results of fluid flow velocity

OPP	CSU:OPP	Group decision (%)	Unit decision (%)	Group decision/unit decision
Cyberoos2001	3:0	71.5	28.5	2.51
FCPortugal2001	1:0	68.4	31.6	2.16
Gemini	26:0	59.7	40.3	1.48
Harmony	3:0	69.9	30.1	2.32
Lazarus	11:0	57.3	42.7	1.34
MRB	2:0	63.2	32.8	1.93
SBCe	4:1	65.8	34.2	1.92
UvA_Trilearn_2001	1:0	54.9	44.1	1.24
UTUtd	10:0	70.7	29.3	2.41
WrightEagle2001	3:1	66.2	33.8	1.96
Average		64.8	35.2	1.84

Table 3   Results of wall shear stress

OPP	CSU:OPP	Group decision (%)	Unit decision (%)	Group decision/unit decision
Cyberoos2001	3:0	71.5	28.5	2.51
FCPortugal2001	1:0	68.4	31.6	2.16
Gemini	26:0	59.7	40.3	1.48
Harmony	3:0	69.9	30.1	2.32
Lazarus	11:0	57.3	42.7	1.34
MRB	2:0	63.2	32.8	1.93
SBCe	4:1	65.8	34.2	1.92
UvA_Trilearn_2001	1:0	54.9	44.1	1.24
UTUtd	10:0	70.7	29.3	2.41
WrightEagle2001	3:1	66.2	33.8	1.96
Average		64.8	35.2	1.84

Table 4   Results of wall pressure

OPP	CSU:OPP	Group decision (%)	Unit decision (%)	Group decision/unit decision
Cyberoos2001	3:0	71.5	28.5	2.51
FCPortugal2001	1:0	68.4	31.6	2.16
Gemini	26:0	59.7	40.3	1.48
Harmony	3:0	69.9	30.1	2.32
Lazarus	11:0	57.3	42.7	1.34
MRB	2:0	63.2	32.8	1.93
SBCe	4:1	65.8	34.2	1.92
UvA_Trilearn_2001	1:0	54.9	44.1	1.24
UTUtd	10:0	70.7	29.3	2.41
WrightEagle2001	3:1	66.2	33.8	1.96
Average		64.8	35.2	1.84

(a) Maximal fluid flow velocity

(b) Average fluid flow velocity

Fig. 6   Fluid flow velocity for DS, FS and NSat at viscosity of 1.45×10^{-3} Pas and inletvelocity of $1\,\mu\mathrm{m/s}$, $10\,\mu\mathrm{m/s}$, $100\,\mu\mathrm{m/s}$ and $1000\,\mu\mathrm{m/s}$

(a) Maximal wall shear stress

(b) Average wall shear stress
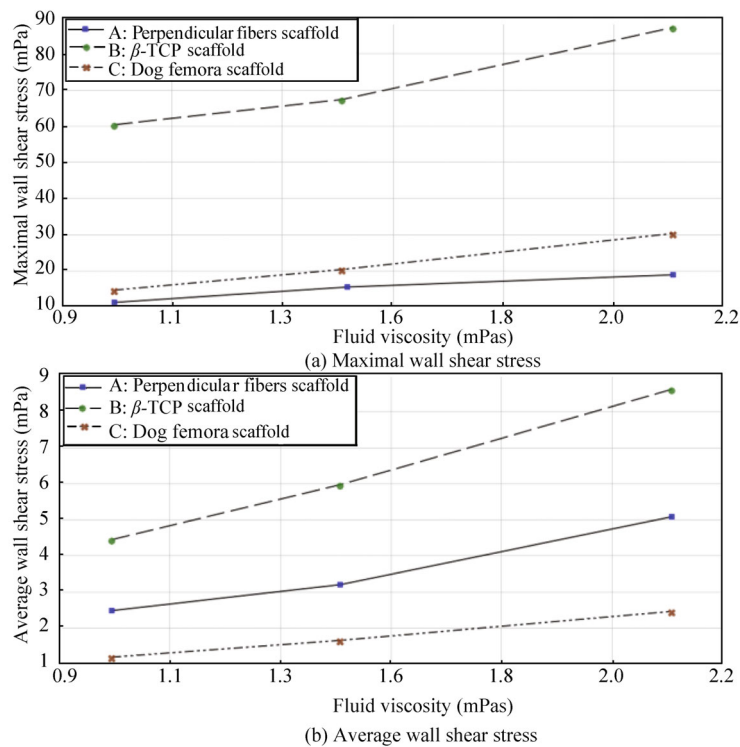
Fig. 7   Wall shear stress for DS, FS and NS at inlet velocity $100\,\mathrm{m/s}$ and viscosity 1.003×10^{-3} Pas, 1.45×10^{-3} Pas and 2.1×10^{-3} Pas

(a) Maximal wall shear stress

(b) Average wall shear stress
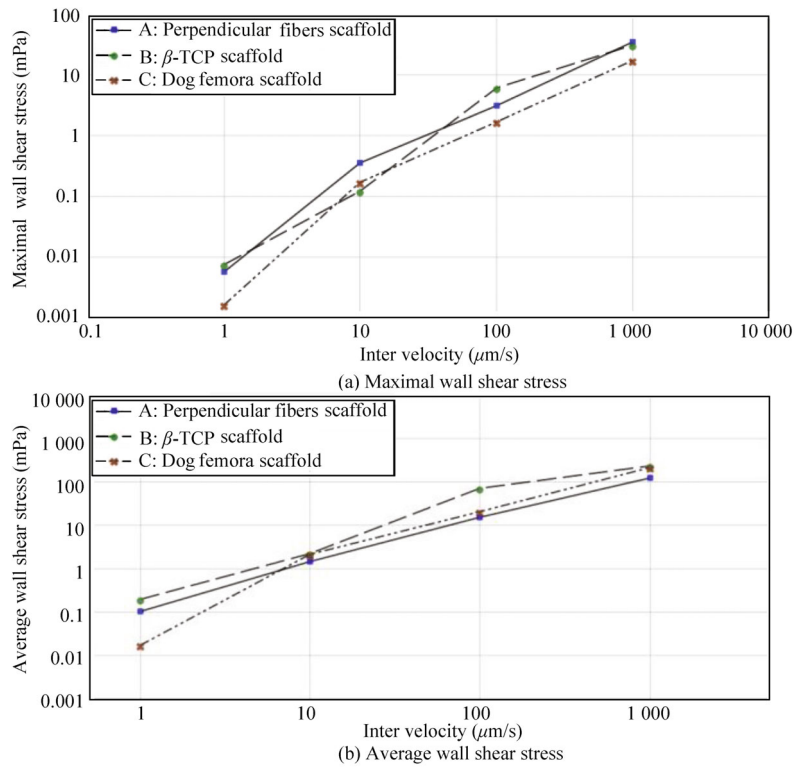
Fig. 8   Wall shear stress for DS, FS and NS at viscosity 1.45×10^{-3} Pas and inletvelocities $1\,\mu m/s$, $10\,\mu m/s$, $100\,\mu m/s$ and $1000\,\mu m/s$

The main distribution of the wall stress was within $10\,\%$ of the maximum, which is shown in Figs. 9 and 10. Both the histograms and contours show that the distribution of wall shear stress is highly matched in FS and NS. Compared to DS, the microstructure and the distribution of wall shear stress in FS and NS were more suitable for perfusion cultivation.

Wall pressures for DS, FS and NS were calculated at 4 levels of inlet velocity and 3 levels of fluid viscosity. The maximal and average wall pressures are presented in Table 4.

As the inlet velocity and viscosity increased, the maximal and average pressures in these 3 kinds of scaffold model all increased. From Fig. 11, the maximal and average wall pressures in FS were larger than those in DS and NS at the same inlet velocity and viscosity. Curves B and C remained parallel, which indicated that these distributions of pressure in FS and NS were similar. It meant that FS and NS had very similar microscopic structures.

4   Discussion

The DS, FS and NS were reconstructed in this study. These 3 samples were simulated in perfusion conditions. The distributions of fluid flow velocity, wall shear stress and pressure were obtained and analyzed. The dog femora scaffold (NS) was regarded as a reference criterion, and the other two samples were used for comparison.

The structure of DS was quite regular with homoge-

neous microscopic characteristics, which resulted in gradient distribution of fluid flow velocity, wall shear stress and pressure[20, 21]. The distribution of fluid flow velocity, wall shear stress and pressure in FS was multifarious resulting from the inhomogeneous microstructure, which was close to that of NS and compatibly used instead of natural bone. At the same initial condition, the fluid flow velocity and wall

(a) The main wall shear stress distribution of DS

(b) The main wall shear stress distribution of FS
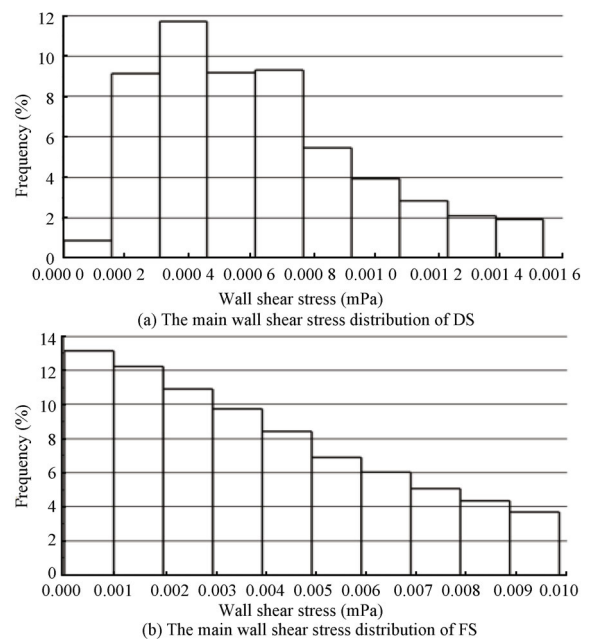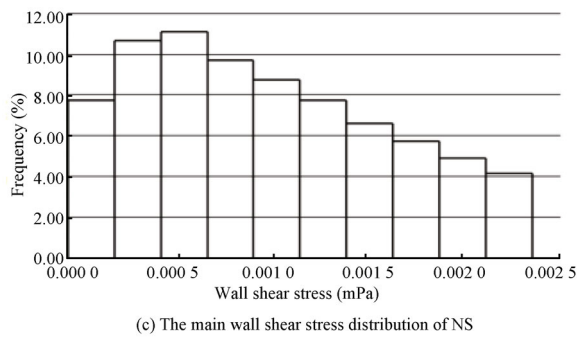
(c) The main wall shear stress distribution of NS

Fig. 9   Scaffolds′ main wall shear stress distribution at viscosity 1.45×10^{-3} Pas and inlet velocity $100\,\mu\mathrm{m/s}$
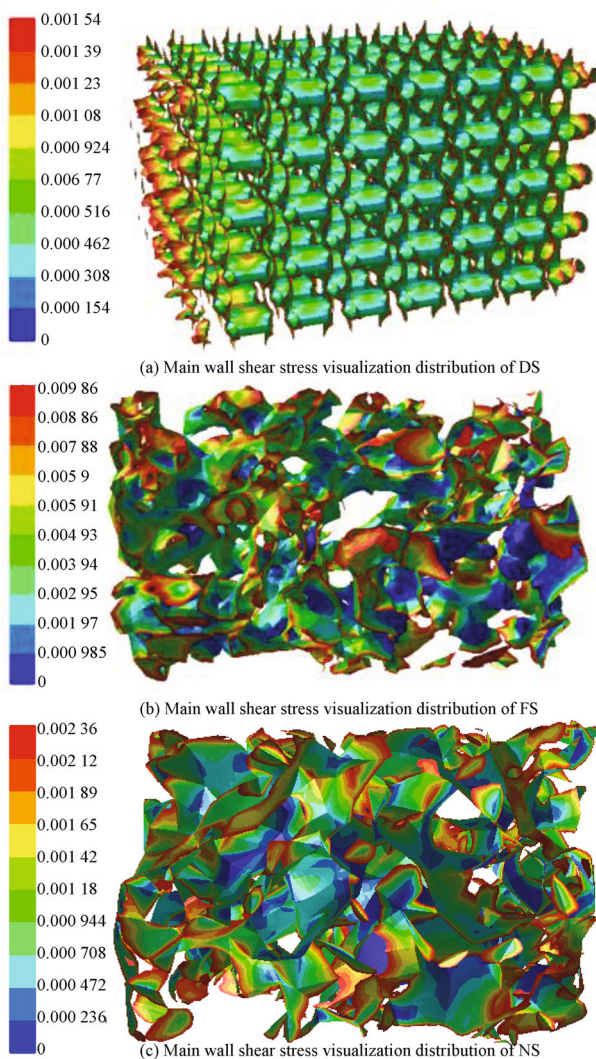
(a) Main wall shear stress visualization distribution of DS

(b) Main wall shear stress visualization distribution of FS

(c) Main wall shear stress visualization distribution of NS

Fig. 10   Scaffolds′ main wall shearstress visualization distribution at viscosity 1.45×10^{-3} Pas and inlet velocity $100\,\mu\mathrm{m/s}$

pressure in FS were a little more than those in NS possibly due to the bad guidance quality of the microstructure.

The maximal and average wall shear stresses in FS were very different from those in NS, which may be a result of too many locally small pores and poor connectivity associated with the freeze-drying process. Compared to FS, the maximal and average wall shear stresses in DS were closer to those in NS. However, the single structure was unfavorable for the cultivation of cells[22]. From Fig. 7, with the inlet velocity increased (from $1\,\mu\mathrm{m/s}$ to $1000\,\mu\mathrm{m/s}$), the maximal and average wall shear stresses in NS linearly increased, which indicated that the favorable microstructure retained the complexity of the formation and the stable flow field environment.
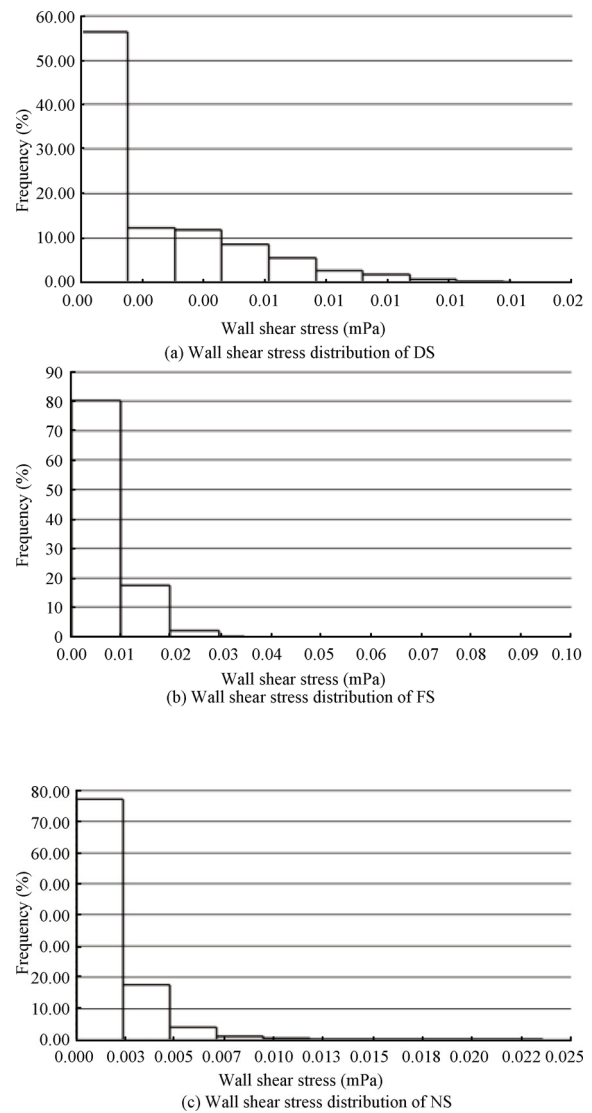
(a) Wall shear stress distribution of DS

(b) Wall shear stress distribution of FS

(c) Wall shear stress distribution of NS

Fig. 11   Scaffolds′ wall shear stress distribution at viscosity 1.45×10^{-3} Pas and inlet velocity $100\,\mu\mathrm{m/s}$

These models consisted of tetrahedral element meshes as irregular microstructures. Seven boundary layers (the first minimum layer thickness was 0.002 mm) based on a growth ratio of 1.2 on the surface of the scaffold models which cell mainly perch were made to capture the distribution of fluid flow velocity and wall shear stress. When the size of bone defects is 3 mm, the body finds it difficult to repair itself. We chose a model where one dimension was 3 mm, which
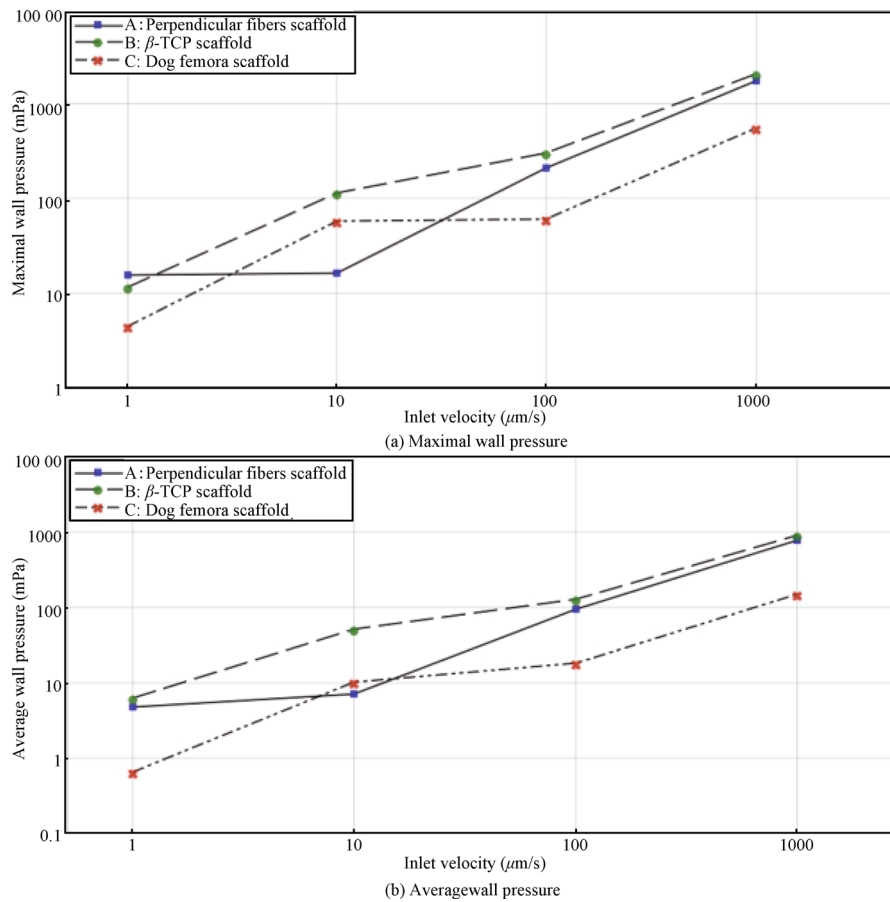
Fig. 12　Scaffolds′ wall pressure at viscosity of 1.45×10^{-3} Pas and inlet velocity of $1\,\mu m/s$, $10\,\mu m/s$, $100\,\mu m/s$ and $1000\,\mu m/s$

can be more powerful for obtaining accurate results. As the computer resource was limited, 0.05 mm elements were decided upon and nearly 1 000 000 elements were created.

In this study, biological conditions were not included in these models. Cell migration, proliferation and differentiation were not simulated. Because of the irregular microstructure of the models, each region in the pores will have a different combination of fluid flow velocity, wall shear stress and pressure. Cells migrate into the scaffolds by means of the interstitial fluid flow. They do not reach the pores where the fluid flow does not penetrate. Abrupt changes of fluid flow velocity, wall shear stress and pressure will be perceived by cells during the migration process. Once cells are seeded in the scaffold, they can attach to specific areas of a pore, according to the mechanical stimuli of each point. However, as cells tend to differ, they synthesize an extracellular matrix and the number of cells increases, which lead to an increase in the fluid viscosity[23]. In this study, the analyzed fluid viscosity was 2.1×10^3 Pas.

A linear relationship between wall shear stress and imposed flow was found as a result of the very low Reynolds numbers causing the convective terms in the Navier-Stokes equations to be negligible[24]. A Newtonian fluid in the steady state was simulated in this study. None penetration wall model and a gravity condition were set. In this study,

we reconstructed the nature of the real bone scaffold model, carried out the flow field analysis, set up 4 levels of inlet velocity, made a comprehensive analysis and compared these 3 models. From Fig. 9, considering the distribution of the wall shear stress for the conditions of 100 m/s inlet velocity and 1.45×10^{-3} Pas viscosity, the wall shear stress was within 0.015 4 Pa in DS, 0.098 5 Pa in FS and 0.023 6 Pa in NS, which were in good agreement with relevant literature[25]. The highest cell viability and proliferation were obtained at an average wall shear stress of 0.05 mPas. An upregulation of osteo-related gene messenger ribouncleic acid (mRNA) was observed as the fluid flow velocity increased from 0.005 to 0.1 mm/s leading to a wall shear stress of 5 mPas, detrimental to cell viability. These results demonstrated that cells can be stimulated by an average wall shear stress of around 1 mPas[23, 26]. From Table 3, at an inlet velocity of $100\,\mu m/s$, for 3 values of viscosity, the average wall shear stress in NS was 1.167 mPas, 1.629 mPas and 2.434 mPas, which was favorable for cell viability, while the corresponding values were 2.493 mPas, 3.223 mPas and 5.099 mPas in DS and 4.426 mPas, 5.494 mPas and 8.601 mPas in FS. The inlet velocity in DS and FS needed to be reduced to obtain an average wall shear stress of around 1 mPas at the expense of cell seeding efficiency[27].
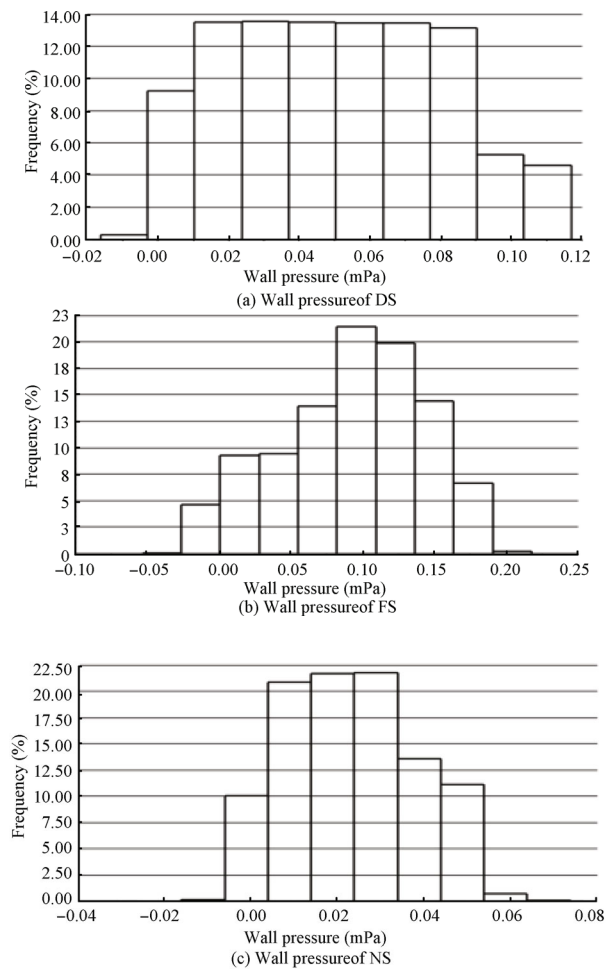
Fig. 13 Scaffolds′ wall pressure at viscosity distribution 1.45×10^{-3} Pas and inlet velocity $100\,\mu\mathrm{m/s}$

5 Conclusions

We have transformed one 3D designed geometry and 2 geometries reversed from micro-CT to meshed models suitable for CFD simulations. This study provided detailed information about mechanical stimuli within the internal walls of these 3 biomaterial scaffolds with different morphologies. Fluid flow velocity, wall shear stress and pressure were determined for different conditions within the scaffolds according to the architecture of the samples suggesting that cells would be exposed to different stimulations. The dog femora scaffold as a reference standard, the designed scaffold and the porous and biodegradable β-TCP based on freeze-drying scaffold were evaluated in terms of microstructure and fluid simulation results. Actually, cell migration, proliferation and differentiation gradually changed the morphology of the scaffold and viscosity of the medium, which could be taken into account in future works. A dynamic perfusion system could be made and future experiments would be necessary. This methodology allowed us to obtain more insight into the complex concept of tissue engineering and will likely help in understanding and eventually improving scaffold design methods.
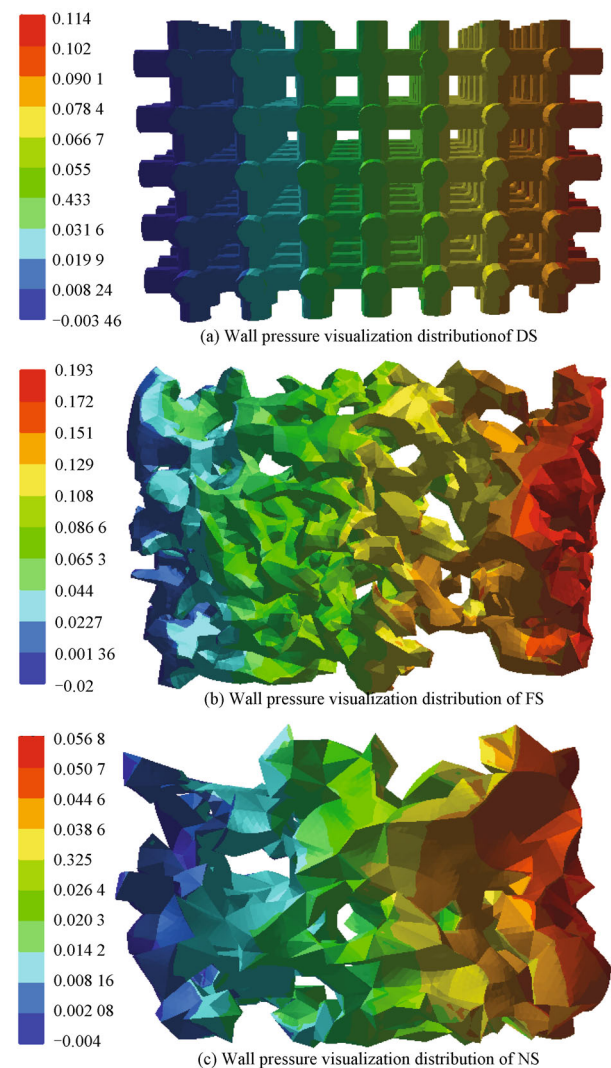
Fig. 14 Scaffolds′ wall pressure visualization distribution at viscosity 1.45×10^{-3} Pas and inlet velocity $100\,\mu\mathrm{m/s}$

References

[1] T. A. Einhorn. Clinically applied models of bone regeneration in tissue engineering research. *Clinical Orthopaedics and Related Research*, vol. 367S, pp. S59–S67, 1999.

[2] H. Petite, V. Viateau, W. Bensaïd, A. Meunier, C. de Pollak, M. Bourguignon, K. Oudina, L. Sedel, G. Guillemin. Tissue-engineered bone regeneration. *Nature Biotechnology*, vol. 18, no. 9, pp. 959–963, 2000.

[3] J. T. Schantz, S. H. Teoh, T. C. Lim, M. Endres, C. Xu Fu Lam, D. W. Hutmacher. Repair of calvarial defects with customized tissue-engineered bone grafts I. Evaluation of osteogenesis in a three-dimensional culture system. *Tissue Engineering*, vol. 9, no. S1, pp. 113–126, 2004.

[4] M. Sittinger, J. Bujia, N. Rotter, D. Reitzel, W. W. Minuth, G. R. Burmester. Tissue engineering and autologous transplant formation: Practical approaches with resorbable biomaterials and new cell culture techniques. *Biomaterials*, vol. 17, no. 3, pp. 237–242, 1996.

[5] P. Giannoni, M. Mastrogiacomo, M. Alini, S. G. Pearce, A. Corsi, F. Santolini, A. Muraglia, P. Bianco, R. Cancedda. Regeneration of large bone defects in sheep using bone marrow stromal cells. *Journal of Tissue Engineering and Regenerative Medicine*, vol. 2, no. 5, pp. 253–262, 2008.

[6] C. K. Griffith, C. Miller, R. C. A. Sainson, J. W. Calvert, N. L. Jeon, C. C. W. Hughes, S. C. George. Diffusion limits of an in vitro thick prevascularized tissue. *Tissue Engineering*, vol. 11, no. 1–2, pp. 257–266, 2005.

[7] A. S. Goldstein, T. M. Juarez, C. D. Helmke, M. C. Gustin, A. G. Mikos. Effect of convection on osteoblastic cell growth and function in biodegradable polymer foam scaffolds. *Biomaterials*, vol. 22, no. 11, pp. 1279–1288, 2001.

[8] E. A. Botchwey, M. A. Dupree, S. R. Pollack, E. M. Levine, C. T. Laurencin. Tissue engineered bone: Measurement of nutrient transport in three-dimensional matrices. *Journal of Biomedical Materials Research Part A*, vol. 67A, no. 1, pp. 357–367, 2003.

[9] J. Glowacki, S. Mizuno, J. S. Greenberger. Perfusion enhances functions of bone marrow stromal cells in three-dimensional culture. *Cell Transplantation*, vol. 7, no. 3, pp. 319–326, 1998.

[10] J. Klein-Nulend, R. G. Bacabac, M. G. Mullender. Mechanobiology of bone tissue. *Pathologie Biologie*, vol. 53, no. 10, pp. 576–580, 2005.

[11] S. M. Mueller, S. Mizuno, L. C. Gerstenfeld, J. Glowacki. Medium perfusion enhances osteogenesis by murine osteosarcoma cells in three-dimensional collagen sponges. *Journal of Bone and Mineral Research*, vol. 14, no. 12, pp. 2118–2126, 1999.

[12] C. R. White, H. Y. Stevens, M. Haidekker, J. A. Frangos. Temporal gradients in shear, but not spatial gradients, stimulate ERK1/2 activation in human endothelial cells. *American Journal of Physiology — Heart and Circulatory Physiology*, vol. 289, no. 6, pp. H2350–H2355, 2005.

[13] K. A. Williams, S. Saini, T. M. Wick. Computational investigation of steady-state momentum and mass transfer in a bioreactor for the production of tissue-engineered cartilage. *Biotechnology Progress*, vol. 18, no. 5, pp. 951–963, 2003.

[14] M. Mullender, A. J. El Haj, Y. Yang, M. A. van Duin, E. H. Burger, J. Klein-Nulend. Mechanotransduction of bone cells in vitro: Mechanobiology of bone tissue. *Medical and Biological Engineering and Computing*, vol. 42, no. 1, pp. 14–21, 2004.

[15] D. P. Byrne, D. Lacroix, J. A. Planell, D. J. Kelly, P. J. Prendergast. Simulation of tissue differentiation in a scaffold as a function of porosity, Young's modulus and dissolution rate: Application of mechanobiological models in tissue engineering. *Biomaterials*, vol. 28, no,36, pp. 5544–5554, 2007.

[16] C. A. Chung, C. W. Chen, C. P. Chen, C. S. Tseng. Enhancement of cell growth in tissue-engineering constructs under direct perfusion: Modeling and simulation. *Biotechnology and Bioengineering*, vol. 97, no. 6, pp. 1603–1616, 2007.

[17] F. Coletti, S. Macchietto, N. Elvassore. Mathematical modeling of three-dimensional cell cultures in perfusion bioreactors. *Industrial & Engineering Chemistry Research*, vol. 45, no. 24, pp. 8158–8169, 2006.

[18] D. J. Wilson, J. R. King, H. M. Byrne. Modelling scaffold occupation by a growing, nutrient-rich tissue. *Mathematical Models and Methods in Applied Sciences*, vol. 17, no. S1, pp. 1721–1750, 2007.

[19] F. Boschetti, M. T. Raimondi, F. Migliavacca, G. Dubini. Prediction of the micro-fluid dynamic environment imposed to three-dimensional engineered cell systems in bioreactors. *Journal of Biomechanics*, vol. 39, no. 3, pp. 418–425, 2006.

[20] A. Oluwajobi, X. Chen. The effect of interatomic potentials on the molecular dynamics simulation of nanometric machining. *International Journal of Automation and Computing*, vol. 8, no. 3, pp. 326–332, 2011.

[21] M. Siva Kumar, P. Philominathan. Purcell's swimmer revisited. *International Journal of Automation and Computing*, vol. 9, no. 3, pp. 325–330, 2012.

[22] A. L. Olivares, E. Marsal, J. A. Planell, D. Lacroix. Finite element study of scaffold architecture design and culture conditions for tissue engineering. *Biomaterials*, vol. 30, no. 30, pp. 6142–6149, 2009.

[23] B. D. Porter, A. S. P. Lin, A. Peister, D. Hutmacher, R. E. Guldberg. Noninvasive image analysis of 3D construct mineralization in a perfusion bioreactor. *Biomaterials*, vol. 28, no. 15, pp. 2525–2533, 2007.

[24] M. Cioffi, F. Boschetti, M. T. Raimondi, G. Dubini. Modeling evaluation of the fluid-dynamic microenvironment in tissue-engineered constructs: A micro-CT based model. *Biotechnology and Bioengineering*, vol. 93, no. 3, pp. 500–510, 2006.

[25] B. Porter, R. Zauel, H. Stockman, R. Guldberg, D. Fyhrie. 3-D computational modeling of media flow through scaffolds in a perfusion bioreactor. *Journal of Biomechanics*, vol. 38, no. 3, pp. 543–549, 2005.

[26] S. H. Cartmell, B. D. Porter, A. J. Garca, R. E. Guldberg. Effects of medium perfusion rate on cell-seeded three-dimensional bone constructs in vitro. *Tissue Engineering*, vol. 9, no. 6, pp. 1197–1203, 2003.

[27] M. Charles-Harris, S. del Valle, E. Hentges, P. Bleuet, D. Lacroix, J. A. Planell. Mechanical and structural characterisation of completely degradable polylactic acid/calcium phosphate glass scaffolds. *Biomaterials*, vol. 28, no. 30, pp. 4429–4438, 2007.

Liu-Lan Lin graduated from Hubei University, China in 1996. She received the M. Sc. degree from Hubei University, China in 1999 and the Ph. D. degree from Huazhong Science and Technology University, China in 2004. She is currently an associate professor at School of Mechatronics Engineering and Automation, Shanghai University, China.

Her research interests include 3D printing and biomaterial.

E-mail: linliulan@staff.shu.edu.cn (Corresponding author)

ORCID iD: 0000-0002-5654-7713

Yu-Jie Lu graduated from Jiangsu University of Science and Technology, China in 2009. He received the M. Sc. degree from Shanghai University, China in 2014.

His research interests includes computer simulation and biomaterial.

E-mail: lyj32100@126.com

ORCID iD: 0000-0003-0632-4965

Ming-Lun Fang graduated from Qinghua University, China in 1964. He is currently a tenured professor at School of Mechatronics Engineering and Automation, Shanghai University, China.

His research interests include advanced manufacturing and intelligent robot.

E-mail: etu2122@shu.edu.cn

ORCID iD: 0000-0002-1849-004X